ChemComm
Chemical Communications

Accepted Manuscript

This article can be cited before page numbers have been issued, to do this please use: J. Wang, G. B. Hwang, C. E. Knapp and D. W. N. Wilson, *Chem. Commun.*, 2024, DOI: 10.1039/D4CC04798B.

ROYAL SOCIETY OF CHEMISTRY

rsc.li/chemcomm

ChemComm

View Article Online
DOI: 10.1039/D4CC04798B

COMMUNICATION

Reversible CO_2 insertion into the silicon-nitrogen σ-bond of an N-heterocyclic iminosilane‡

Received 00th January 20xx,
Accepted 00th January 20xx

DOI: 10.1039/x0xx00000x

Jingyan Wang,[a] Gi Byoung Hwang,[a] Caroline E. Knapp,[a] Daniel W. N. Wilson.[a*]

The reversible insertion of carbon dioxide into the silicon-nitrogen bond of an N-heterocyclic iminosilane is reported. Solution-phase thermodynamic investigations indicate that this process is thermoneutral and reversible, whereas in the solid-phase CO_2 can be stored for extended periods and is only released upon heating to 133°C.

The rising atmospheric concentration of the greenhouse gas carbon dioxide (CO_2) is an urgent pressing global concern. New technologies for the capture, storage, or valorization of CO_2 from flu gas or directly from the air help mitigate the detrimental effects of CO_2 atmospheric accumulation.[1,2] The ability to reversibly bind and store CO_2 through the formation of weak, easily breakable chemical bonds creates energetically efficient carbon fixation pathways.[3] Additionally, such potential energy landscapes are ideal for the development of catalysts which can convert CO_2 into industrially useful feedstocks.[4] Technologies based on earth abundant elements would provide a sustainable route to CO_2 utilization.[5] A variety of low-valent transition metal (TM) and p-block Lewis bases can coordinate to the electrophilic carbon of CO_2 to form zwitterionic complexes.[6] Amongst these, nitrogen bases are particularly desirable due to their low cost and ease of synthetic access (Figure 1; A). Amidine- and guanidine-derived superbases bind CO_2 weakly and can catalyse its reduction to a variety of products, including amide and methanol-precursors.[6–10] Recently, a range of N-heterocyclic imides have been reported which can capture CO_2 and release it upon heating or photolysis, highlighting their potential use for CO_2 storage.[11,12]

In addition to Lewis acid-base complexes, CO_2 can insert into homo- and hetero-element σ-bonds.[13,14] The best studied systems in this class feature late TM–E bonds, where E can be a hydride or p-block element (Figure 1; B. E = H, OR, NR_2, CR_3, SiR_3), in which CO_2 insertion is an elementary step preceding CO_2 valorization.

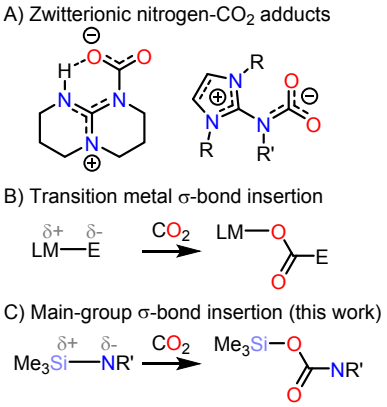

Figure 1. A) Previous examples of nitrogen-bases which coordinate CO_2. B)The insertion of CO_2 into transition metal (M)-heteroatom (E) bonds (L = ligand). C) This work: The reversible insertion of CO_2 into a nitrogen-silicon bond.

The insertion of CO_2 into earth abundant and inexpensive p-block element-element bonds would provide an alternative to TMs, however such insertions typically yield thermodynamically stable products which do not easily release CO_2, and requiring catalytic strategies with large driving forces (e.g. high temperatures).[6] Examples of reversible CO_2 activation by p-block complexes include bonds between divalent group 14 elements, Ge^{2+}–Ge^{2+} and Sn^{2+}–Sn^{2+},[15] and select Lewis acid-base adducts (including Sn–P, In–P, N–Al complexes) which can dissociate to capture CO_2.[16–18] In these cases, high temperatures and reduced pressures are needed to induce loss of CO_2, rendering them incompatible to thermodynamic study requiring closed systems and limiting the understanding of their mechanisms.

Here, we report the reversible, thermoneutral capture of CO_2 by a N–Si bond. The solution phase thermodynamic parameters for the insertion reaction were determined by variable temperature NMR experiments, and the mechanism was further elucidated using density functional theory

[a] *Department of Chemistry, University College London, 20 Gordon Street, London, UK.*

‡ Data for this article, including experimental procedures, computational details, crystallographic data and NMR spectra are available at [{placeholder URL}]. The data supporting this article have been included as part of the Supplementary Information. Crystallographic data for **1** has been deposited at the CCDC under 2384340 (**1**).

calculations. Thermogravimetric analysis indicates that CO_2 can be stored in the solid state up to 133 °C, at which point reformation of the starting material occurs. Contrasting this, dissolution of the solids results in release of CO_2 under ambient conditions, presenting a novel route to molecular CO_2 storage.

N-heterocyclic imines typically bind CO_2 through coordination of the imine nitrogen to the electrophilic CO_2 carbon, forming zwitterionic acid-base adducts.[11,12] The steric and electronic properties of the NHC have been shown to affect the binding energy of the N–CO_2 bond.[11] However, there has been little exploration of how modifying the imine substituent influences reactivity. We hypothesized that modifying the electropositivity, oxophilicity, and/or covalency of the imine subsituent would allow for sigma-bond insertions analogous to those observed in TM–E compounds.[13] Exposure of a benzene solution of **IPrNSiMe$_3$**[19] (IPr = 1,3-di(2′,6′-diisopropylphenyl)imidazolin-2-ylidene) to CO_2 (1 Bar; Scheme 1) results in the appearance of new resonances in the ^{1}H NMR spectrum alongside the resonances associated with the starting material (Figure S2). Neither addition of further CO_2 nor heating resulted in complete conversion to the product, and removal of the CO_2 gas from the headspace of the reaction resulted in a loss of intensity of the resonances associated with the product concomitant with an increase in intensity for the **IPrNSiMe$_3$** resonances, consistent with a reversible reaction. Performing the reaction in hexane, a low polarity solvent, at –35°C allowed for the isolation of analytically pure, colourless crystals of $IPrNCO_2SiMe_3$ (**1**, isolated in 76% yield).

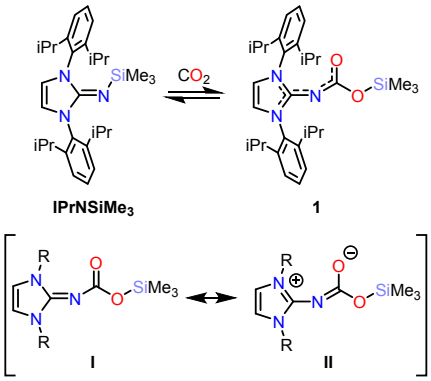

Scheme 1. Top: Equilibrium between **IPrNSiMe$_3$** and **1**. Bottom: Neutral (I) and zwitterionic (II) resonance structures of **1** (R = 2,6-diisopropylphenyl).

The crystal structure of **1** (Figure 2; top) revealed CO_2 insertion into the N–Si bond of **IPrNSiMe$_3$**, rather than formation of an acid-base adduct as observed in previous studies on alkyl-substituted N-heterocyclic imines.[11,12] The C1–N1 distance is 1.319(2) Å, elongated with respect to the precursor (c.f. 1.265(3) Å)[19] indicating reduced double bond character with respect to **IPrNSiMe$_3$**. The N1–C2 distance is 1.3434(15) Å, falling within the expected distance for single (1.46 Å)[20] and double bonds (1.27 Å), in line with contribution from both the neutral (Scheme 1; **I**) and zwitterionic (**II**) resonance structures of **1**. The C2–O1 and C2–O2 bonds are C2 1.3636(14) and 1.2272(15) Å, respectively, slightly contracted with respect to the expected distance for single (1.38 Å) and double (1.24 Å) bonds. Despite significant delocalization throughout the conjugated atoms, which would benefit from planarity to maximise overlap between π-orbitals, the NCO_2SiMe_3 moiety is twisted out of the NHC plane by 47°. This is likely due to steric hinderance of the diisopropylphenyl groups.

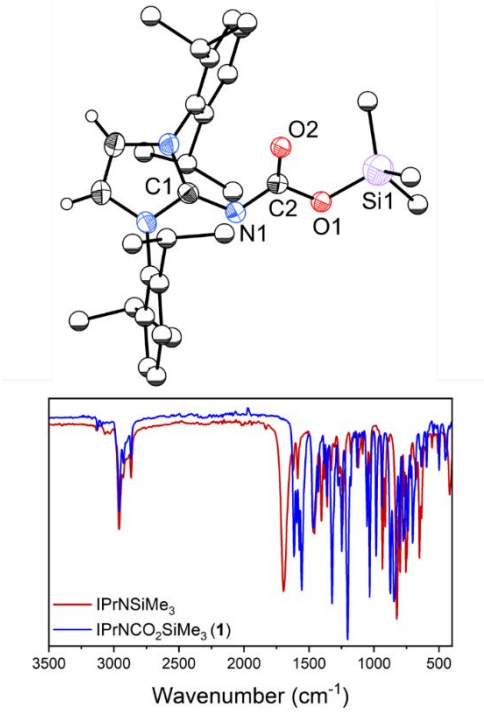

Figure 2. Top: Crystral structure of **1**. The thermal elipsoids are drawn at 50% probability. The diisopropyl and methyl carbon atoms are shown as spheres or arbitrary radius, and most hydrogen atoms are ommitted for clarity. Key bond lengths (Å) and angles (°): C1–N1, 1.3187(15); N1–C2, 1.3434(15); C2–O2, 1.2272(15); C2–O1, 1.3636(14); O1–Si1, 1.6712(9). C1-N1-C2, 119.80(10); N1-C2-O1, 110.87(10); O2-C2-N1 128.96(11); O2-C2-O1, 120.09(11). Bottom: FTIR spectra of $IPrNSiMe_3$ (red) showing strong absorption at 1695 cm^{-1} and **1** (blue) showing new absorptions at 1613 and 1558 cm^{-1}.

Fourier-transform infrared (FTIR) analysis performed on crystalline **1** was consistent with complete consumption of **IPrNSiMe$_3$**, evidenced by the loss of the diagnostic carbonic C_{NHC}=N stretch at 1695 cm^{-1} (Figure 2). New stretches at 1613 and 1558 cm^{-1} were present in the spectrum of **1**, which we assign as the C_{NHC}=N stretch and the CO_2 asymmetric stretch, respectively, the former is in keeping with the reduction of C_{NHC}–N bond order observed in the solid state, and further supports contribution from the zwitterionic resonance structure. Dissolving the crystals of **1** resulted in the reappearance of **IPrNSiMe$_3$** in the ^{1}H NMR spectrum, and leaving the system open to atmosphere or applying vacuum converts the mixture to **IPrNSiMe$_3$**, indicating that the two species are in equilibrium. While p-block systems capable of CO_2 capture are known,[21–23] there are few examples of reversible CO_2 capture,[15–17] and fewer still are amenable to mechanistic study.[24,25] Because of the reversibility of CO_2 binding under ambient conditions, **IPrNSiMe$_3$** presents an ideal platform for such study.

The presence of well-defined and unbroadened ^{1}H NMR resonances for **IPrNSiMe$_3$** and **1** indicates slow chemical

View Article Online
DOI: 10.1039/D4CC04798B

exchange with respect to the NMR timescale (500 MHz). Variable temperature (VT) NMR studies performed on a solution of **IPrNSiMe$_3$** under 1 bar of CO_2 allowed for the determination of thermodynamic parameters for the equilibrium ($\Delta H°$, $\Delta S°$, and $\Delta G°$) by linear regression of the van't Hoff plot of ln(K_{CO2}) vs 1/T (Figure 3). Giving value of $\Delta H°$ = –61 ± 1 kJ mol^{-1}, $\Delta S°$ = –194 ± 4 J mol^{-1}, and $\Delta G°$ = –3.3 ± 0.1 kJ mol^{-1}. The reaction is overall slightly endergonic, with a relatively large negative enthalpy, consistent with the formation of new N–C and O–Si bonds, and a negative entropy as expected from a condensation reaction.

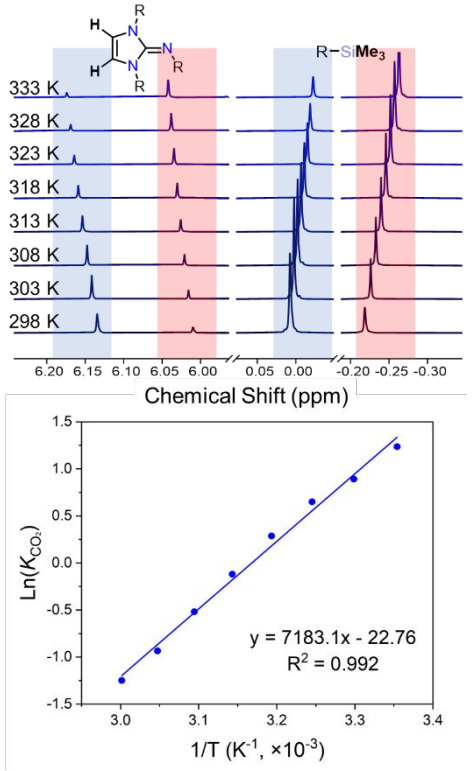

Figure 3. Top: Variable temperature ^{1}H NMR (500 MHZ, toluene-d$_8$, 298-333 K) studies under 1 Bar CO_2. Region highlighted blue corresponds to resonances associated with **1**, while red corresponds to **IPrNSiMe$_3$**. Bottom: van't Hoff plot of Ln(K_{CO2}) vs 1/T.

Self-exchange rates were extracted from the VT NMR analysis.[26] Due to the slow rate of equilibrium, no line broadening was observed and the rate of exchange between **1** and **IPrNSiMe$_3$** was determined from the integration of NMR peaks. We propose the mechanism of interconversion of **1** + **IPrNSiMe$_3$** ⇌ **IPrNSiMe$_3$** + **1** occurs via dissociation of CO_2 from **1**, followed by association of CO_2 to **IPrNSiMe$_3$** (Figure S7), where the rate limiting step is the dissociation of CO_2 (k_{loss}) (See SI section 4.0). Eyring plots of ln(k_{loss}/T) vs 1/T (Figure S8) allowed for the determination of activation parameters of CO_2 loss: $\Delta H^‡_{loss}$ = +32 ± 0.6 kJ mol^{-1}, $\Delta S^‡_{loss}$ = –95 ± 24 J mol^{-1} and $\Delta G^‡_{loss}$ = +61 ± 7 kJ mol^{-1}. Further, from the relationship $\Delta G^‡_{loss} = \Delta G^‡_{bind} - \Delta G°$, $\Delta G^‡_{bind}$ can be estimated as +64 ± 7 kJ mol^{-1}.

Density functional theory (DFT) calculations were performed to gain further insight into the mechanism of CO_2 binding. A variety of basis sets and functional combinations were screened (See SI 8.0).[27,28] Notably, the thermodynamics of the reaction were highly dependent on the method employed. Pople basis sets resulted in highly exergonic reactions with reverse barriers too large to be reversible at room temperature (e.g. for PBE/6311++g-D3 ΔG_{calc} = –55 kJ mol^{-1}, $\Delta G^‡_{reverse}$ = +131 kcal mol^{-1}). The method BP86/def2-TZVP-D3 gave forward (+71 kJ mol^{-1}) and reverse (+73 kJ mol^{-1}) energetic barriers which were slightly overestimated with respect to the experimentally determined barrier (c.f. +64 ± 7 kJ mol^{-1}) however qualitatively reproduces the reaction energetics (Figure 4). An energetically reasonable mechanism involves initial coordination of CO_2 to the imine to form the zwitterionic intermediate (**Int1**). Contrasting previously reported and isolable N-heterocyclic imine–CO_2 adducts, **Int1** is significantly higher in energy than the starting molecules (+68 kcal mol^{-1}), possibly due to steric clash between the diisopropylphenyl groups and the CO_2 moiety.[11] The energetic barrier between **Int1** and **1** is small (12 kJ mol^{-1}) and proceeds via a 4-membered transition state (**TS2**) in which the silyl group migrates from the nitrogen to the oxygen. The overall reaction, **IPrNSiMe$_3$** + CO_2 → **1**, is slightly endergonic (ΔG_{calc} = +11 kJ mol^{-1}), contrasting the experimentally determined $\Delta G°$ = –3.3 ± 0.1 kJ mol^{-1}. The difference between experimental and computational free energy is small and is likely due to errors associated with the methodology employed, which even in the best case can be as much as 8 kJ mol^{-1},[27] and the limitations of DFT in accurately accounting for the entropy associated with solvating gas-phase molecules, in this case CO_2.[29]

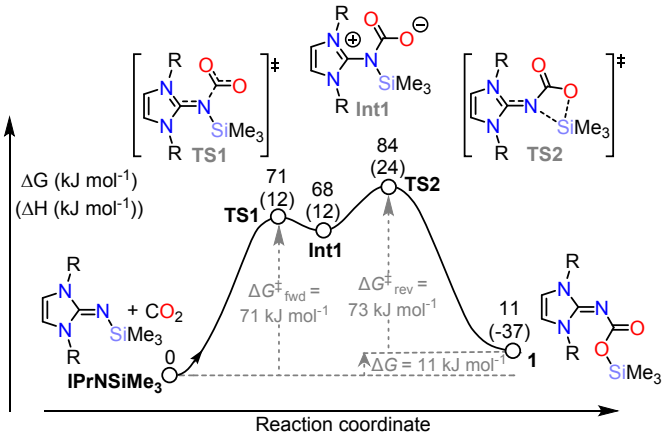

Figure 4. Calculated reaction mechanism and potential energy surface (in kJ mol^{-1}) for the conversion of **IPrNSiMe$_3$** to **1**. Method: BP86/def2-TZVP-D3 with the application of a continuum solvation model to mimic the effect of benzene solvent. R = 2,6-diisopropylphenyl.

Reducing the steric bulk at the N-heterocyclic carbene moiety in the calculated models (Dipp → Me; PBE//6311g++/D3) did not impact the qualitative reaction profile, with **Int1^{Me}** significantly higher in energy in comparison to reactants and products ($\Delta G^‡$ = +44 kcal mol^{-1}, ΔG_{calc} = +6 kJ mol^{-1}). This indicates that the electropositivity and propensity for migration of silane in comparison to carbon substituents facilitates the migration, rather than the reaction being driven by release of steric clash.

Having established the solution-phase behaviour of **1**, we sought to assess if **1** could store and release CO_2 in the solid

state. Thermogravimetric analysis on crystalline **1** revealed two features, a sharp decrease at 133 °C followed by a broad feature beginning after 200 °C and centered at 347 °C (Figure 6). Plotting the first derivative of the curve revealed two separate events, with the area under the first peak integrating as 8.7% of the total sample mass, in agreement with the theoretical mass of CO_2 in the sample (8.5%). FTIR analysis of crystals of **1** heated to 140°C showed loss of the absorbances associated with the CO_2 stretch and reappearance of the peak at 1695 cm^{-1}. Dissolving the resultant solids displayed the diagnostic ^1H NMR resonances associated with **IPrNSiMe$_3$**. Therefore, in the solid-state CO_2 is released and **IPrNSiMe$_3$** can be reformed. The temperature at which **1** releases CO_2 is higher than those reported for N-heterocyclic imine-CO_2 adducts, which decarboxylate between 30 and 100 °C, depending on the identity of the NHC moiety and its substituents.[11]

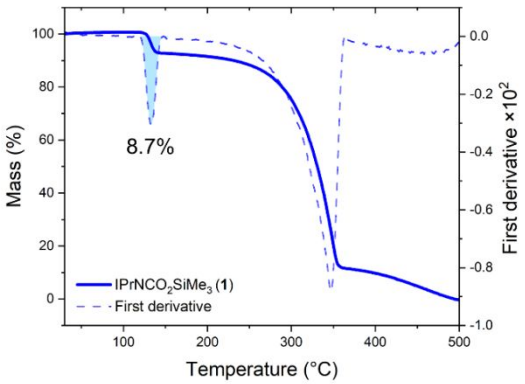

Figure 5. Thermogravimetric plot for **1** (solid line), and its first derivative (dashed line). Shaded blue area shows the area integrating as 8.7% of total sample mass.

In summary, we have demonstrated the capture of CO_2 by an N-heterocyclic iminosilane. In the solution-phase, NMR experiments demonstrate that this reaction is almost thermoneutral and fully reversible, while in the solid-state CO_2 can be stored for extended periods up to 133 °C. Computations indicate that the reversibility of this reaction is due to the oxophilicity of the silane substituent.

Conflicts of interest

There are no conflicts to declare.

Data availability

The data supporting this article have been included as part of the ESI.† Raw data for each experiment can be obtained by contacting the corresponding author.

Notes and references

1 M. Aresta, A. Dibenedetto and A. Angelini, *Chem. Rev.*, 2014, **114**, 1709–1742.
2 E. S. Sanz-Pérez, C. R. Murdock, S. A. Didas and C. W. Jones, *Chem. Rev.*, 2016, **116**, 11840–11876.
3 L. J. Murphy, K. N. Robertson, R. A. Kemp, H. M. Tuononen and J. A. C. Clyburne, *Chem. Commun.*, 2015, **51**, 3942–3956.
4 L. Zhao, H.-Y. Hu, A.-G. Wu, A. O. Terent'ev, L.-N. He and H.-R. Li, *Journal of CO_2 Utilization*, 2024, **82**, 102753.
5 K. M. P. Wheelhouse, R. L. Webster and G. L. Beutner, *Org. Process Res. Dev.*, 2023, **27**, 1157–1159.
6 S. P and S. K. Mandal, *Chemical Science*, 2020, **11**, 10571–10593.
7 C. Villiers, J.-P. Dognon, R. Pollet, P. Thuéry and M. Ephritikhine, *Angew. Chem. Int. Ed.*, 2010, **49**, 3465–3468.
8 C. Das Neves Gomes, O. Jacquet, C. Villiers, P. Thuéry, M. Ephritikhine and T. Cantat, *Angew. Chem. Int. Ed.*, 2012, **51**, 187–190.
9 H. Zhou, W. Chen, J.-H. Liu, W.-Z. Zhang and X.-B. Lu, *Green Chem.*, 2020, **22**, 7832–7838.
10 J. K. Mannisto, L. Pavlovic, T. Tiainen, M. Nieger, A. Sahari, K. H. Hopmann and T. Repo, *Catal. Sci. Technol.*, 2021, **11**, 6877–6886.
11 L. F. B. Wilm, T. Eder, C. Mück-Lichtenfeld, P. Mehlmann, M. Wünsche, F. Buß and F. Dielmann, *Green Chem.*, 2019, **21**, 640–648.
12 L. F. B. Wilm, M. Das, D. Janssen-Müller, C. Mück-Lichtenfeld, F. Glorius and F. Dielmann, *Angew. Chem. Int. Ed.*, 2022, **61**, e202112344.
13 N. Hazari and J. E. Heimann, *Inorg. Chem.*, 2017, **56**, 13655–13678.
14 A. P. Deziel, M. R. Espinosa, L. Pavlovic, D. J. Charboneau, N. Hazari, K. H. Hopmann and B. Q. Mercado, *Chem. Sci.*, 2022, **13**, 2391–2404.
15 A. Caise, L. P. Griffin, C. McManus, A. Heilmann and S. Aldridge, *Angew. Chem. Int. Ed.*, 2022, **61**, e202117496.
16 D. A. Dickie, E. N. Coker and R. A. Kemp, *Inorg. Chem.*, 2011, **50**, 11288–11290.
17 D. A. Dickie, M. T. Barker, M. A. Land, K. E. Hughes, J. A. C. Clyburne and R. A. Kemp, *Inorg. Chem.*, 2015, **54**, 11121–11126.
18 T. W. Yokley, H. Tupkar, N. D. Schley, N. J. DeYonker and T. P. Brewster, *Eur. J. of Inorg. Chem.*, 2020, **2020**, 2958–2967.
19 M. Tamm, S. Randoll, E. Herdtweck, N. Kleigrewe, G. Kehr, G. Erker and B. Rieger, *Dalton Trans.*, 2006, 459–467.
20 P. Pyykkö, *J. Phys. Chem. A*, 2015, **119**, 2326–2337.
21 D. Sarkar, L. Groll, D. Munz, F. Hanusch and S. Inoue, *ChemCatChem*, 2022, **14**, e202201048.
22 F. Gründler, H. Scholz, M. Herbig, S. Schwarzer, J. Wagler and E. Kroke, *Euro. J. of Inorg. Chem.*, 2021, **2021**, 2211–2224.
23 K. Kraushaar, C. Wiltzsch, J. Wagler, U. Böhme, A. Schwarzer, G. Roewer and E. Kroke, *Organometallics*, 2012, **31**, 4779–4785.
24 C. M. Mömming, E. Otten, G. Kehr, R. Fröhlich, S. Grimme, D. W. Stephan and G. Erker, *Angew. Chem. Int. Ed.*, 2009, **48**, 6643–6646.
25 F. Buß, P. Mehlmann, C. Mück-Lichtenfeld, K. Bergander and F. Dielmann, *J. Am. Chem. Soc.*, 2016, **138**, 1840–1843.
26 R. C. Cammarota, J. Xie, S. A. Burgess, M. V. Vollmer, K. D. Vogiatzis, J. Ye, J. C. Linehan, A. M. Appel, C. Hoffmann, X. Wang, V. G. Young and C. C. Lu, *Chem. Sci.*, 2019, **10**, 7029–7042.
27 M. Bursch, J.-M. Mewes, A. Hansen and S. Grimme, *Angew. Chem. Int. Ed.*, 2022, **61**, e202205735.
28 B. A. Shiekh, *ACS Omega*, 2019, **4**, 15435–15443.
29 S.-C. Liu, X.-R. Zhu, D.-Y. Liu and D.-C. Fang, *Phys. Chem. Chem. Phys.*, 2023, **25**, 913–931.

View Article Online
DOI: 10.1039/D4CC04798B

Data for this article, including experimental procedures, computational details, crystallographic data and NMR spectra are available at [{placeholder URL}]. The data supporting this article have been included as part of the Supplementary Information. Crystallographic data for **1** has been deposited at the CCDC under 2384340 (**1**).